SCALING LAWS FOR STRESS AND ENERGY FOR INTERFACE WITH STRONG RATE-WEAKENING FRICTION

BY

YUYANG RAO

THESIS

Submitted in partial fulfillment of the requirements
for the degree of Master of Science in Civil Engineering
in the Graduate College of the
University of Illinois at Urbana-Champaign, 2017

Urbana, Illinois

Adviser:

Professor Ahmed Elbanna

ABSTRACT

In this study, we present a systematic analysis of chaotic behaviors of earthquakes, using a modified Burridge-Knopoff chain model. Velocity weakening friction law is assumed between sliders and rigid surface. Both the statistical properties of slip, pulling force and average rupture stress are studied with varying the constitutive parameters characterizing the model: the stiffness ratio and strength of the velocity-weakening. Longtime investigations suggest that firstly, a pulse-like brittle behavior would likely to happen for stiff springs and a creep (ductile behavior) would likely to happen for weak springs; secondly, heterogeneity is introduced by strong velocity weakening; thirdly, an empirical relation is explored between average rupture stress and slip, specifically the average rupture stress is logarithmically inverse proportional to slip length; lastly, a scaling law for the system nominal strength may be extracted based on the statistical properties of the prestress. We discuss the implications of our model for understanding the chaotic behaviors of systems with multiscale fractures.

ACKNOWLEDGEMENTS

Foremost, I would like to express my sincere gratitude to my advisor Prof. Ahmed Elbanna for the continuous support of my M.S. study and research, for his patience, motivation, enthusiasm, and immense knowledge. His guidance helped me in all the time of research and writing of this thesis. I would like to thank the Department of Civil and Environmental Engineering at University of Illinois at Urbana Champaign for providing the high quality of education courses and academic resources. I am also grateful to all colleagues in our group for offering suggestions and help to my research. Last but not the least, I would like to thank my family: my parents Chengyong Rao and Wen Pang, for inspiration throughout my life.

TABLE OF CONTENTS

CHAPTER 1

INTRODUCTION

Although significant advances have been made in our knowledge of earthquake, our understanding of the physical mechanisms responsible for the initiation, propagation and termination of earthquake rupture remains unclear. Models of fault systems are important for understanding scaling laws, the occurrence of characteristic events, and the relation between small and large earthquakes [Rice, 1993]. In addition to the benefits that would result from understanding earthquake faults, understanding driven dissipative systems is important in physics and related fields. In the 1960s, Burridge and Knopoff (BK) introduced the mechanical block-spring model [Burridge and Knopoff 1967] to simulate interactions between two surfaces of a fault. Since then, simulations of the Burridge-Knopoff model have become an essential tool for understanding the mechanisms of earthquake or other fault systems. This work uses analytical and numerical methods, in discrete modeling frameworks, to study the dynamics of earthquake ruptures propagating on strong velocity-weakening frictional interfaces. Longtime investigations suggest that firstly, a pulse-like brittle behavior would likely to happen for stiff springs and a creep (ductile behavior) would likely to happen for weak springs; secondly, heterogeneity is introduced by strong velocity weakening; thirdly, an empirical relation is explored between average rupture stress and slip, specifically the average rupture stress is logarithmically inverse proportional to slip length; lastly, a scaling law for the system nominal strength may be extracted based on the statistical properties of the prestress. We discuss the implications of our model for understanding the chaotic behaviors of systems with multiscale fractures.

This work also applies the dynamic discrete model to current study of seismicity induced by water injection and hydraulic fracturing. Man-made seismicity refers to typically minor

earthquakes and tremors that are caused by human activity, like wastewater injection and hydraulic fracturing. Hydraulic fracturing and water injection could reduce the pore water pressure and thus, reduce the normal stress which directly related with the velocity weakening friction. In this thesis, we explore the impact of reduced pore water pressure and location of water injection on the size and stress of seismicity.

CHAPTER 2

THEORY AND MODEL SETUP

The spring block slider model was firstly introduced in 1967 by Burridge and model [Burridge and Knopoff (1967), Carlson and Langer (1989), Carlson et al. (1991) and Erickson et al. (2008)] as an idealization of system rupturing at multiple length scale, such as earthquakes. It is a one dimensional dynamic rupture system subject to a friction law and an initial prestress distribution. Simulation of Burridge and Knopoff's chain model provides insightful aspects for exploring statistical properties of one dimensional rupture system, scaling laws of rate weakening friction and understandings on earthquake's self-organization in physics and other related areas. In Burridge and Knopoff's spring block slider model, each block is connected by linear coil springs with their neighbor block and is also connected to a loading plate by linear leaf spring. The blocks rest on a rigid surface subjected to velocity weakening friction force. Once the loading plate starts to move and the force in leaf spring exceeds static friction, a single block would slip. The initial slip of this single block will dissipate energy to its neighboring coil springs, causing movement of other blocks and then, an earthquake event happens. This model is discrete and one dimensional, and thus this model is unrealistic and cannot fully capture the rupture behavior in a continuum media. However, the Burridge and Knopoff's model is an effective tool to understand the statistical properties of rupture slip, rupture stress and event size distribution for large-scale continuum model.

The setup of the spring block slider model is slightly different with Burridge and Knopoff 's spring block model, as shown in Figure 1. Instead of connecting each block to a moving plate by a leaf spring in Burridge and Knopoff 's model, only the first block is connected to a pulling force with an initial velocity (v). The model used for this simulation of fault slip consists of a chain of

N blocks with identical mass (m). Each of the blocks is connected by coil springs with stiffness (k_c) to its neighboring blocks. Once the pulling force exceeds static friction, the first block will move. It will further transfer stresses to its neighboring blocks and causing them to move if the elastic force exceeds static friction. A dynamic friction force ϕ is used to represent the friction between blocks and the surface when the blocks are moving. An event is complete when all the blocks stop sliding.

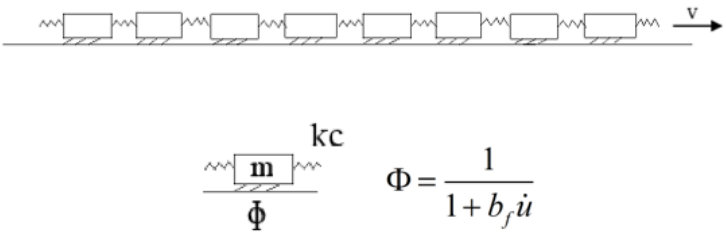

Figure 1: Modified One-dimensional Spring-block-slider Model

Once the static friction is exceeded, the motion of the i^{th} block (u_i) is given by the following differential equation:

$$m_i \ddot{u}_i = k_c(u_{i+1} - 2u_i + u_{i-1}) - \frac{F_{st}}{1+b_f \dot{u}_i} + \sigma_{oi} \quad (2.1)$$

and the motion of the first block ($\boldsymbol{u_1}$) is given by:

$$m_1 \ddot{u}_1 = k_c(u_2 - u_1) - k_l u_1 + k_l v_p t - \frac{F_{st}}{1+b_f \dot{u}_1} + \sigma_{o1} \quad (2.2)$$

and the motion of the last block ($\boldsymbol{u_n}$) is given by:

$$m_n \ddot{u}_n = k_c(u_{n-1} - u_n) - \frac{F_{st}}{1+b_f \dot{u}_n} + \sigma_{on} \quad (2.3)$$

Equation (2.1) represents a set of n ordinary differential equations where n is the number of blocks; each of these ODE's are nonlinear because of the friction term. We use a second order predictor-corrector scheme for solving the equation. The material and frictional properties are

assumed to be spatially homogeneous. The time step is controlled by the ratio of the spring stiffness connected to the pulling force to coil spring stiffness, $r = {k_c}/{k_l}$ and the rate of frictional weakening, b_f. The term σ_{oi} represents the initial traction at the position of the i[th] block. We assume uniform masses, m =1. F_{st} measures local static frictional strength. Equation (2.2) represents the equation of motion for the first block that is connected to a pulling force. The term k_l is the spring stiffness that connect the first block to the pulling force. In this simulation, we consider k_l as 1. The velocity of pulling force is constant, written as v_p. Time t measures the time that the first block is pulled.

In order to write Equation 2.1 to 2.3 into non-dimensional form, we introduce length scale:

$$D = \frac{F_{st}}{k_l} \tag{2.4}$$

and time scale:

$$\tau = \omega t \tag{2.5}$$

where ω is the natural frequency of the first block connected to the pulling spring only:

$$\omega = \sqrt{\frac{k_l}{m}} \tag{2.6}$$

Once we normalize displacement and time by D and τ, we rewrite Equation (2.1) in the following form:

$$\ddot{U}_i = r(U_{i+1} - 2U_i + U_{i-1}) - \frac{1}{1+\frac{\dot{U}_i}{v_c}} + \frac{\sigma_{oi}}{F_{st}} \tag{2.7}$$

rewriting equation (2.2) in the following form:

$$U_1 = r(U_2 - U) - U_1 + \gamma\tau - \frac{1}{1+\frac{\dot{U}_1}{v_c}} + \frac{\sigma_{o1}}{F_{st}} \tag{2.8}$$

and rewriting equation (2.3) by:

$$U_n = r(U_{n-1} - U_n) - \frac{1}{1+\frac{\dot{U}_n}{v_c}} + \frac{\sigma_{on}}{F_{st}} \tag{2.9}$$

In Equation (2.7) to (2.9), r represents the stiffness ratio where $r = {k_c}/{k_l}$. Normalized displacement is U where $U = {u}/{D}$. γ is the normalized loading rate where $\gamma = {v_p}/{\omega D}$ The ratio v_c measures the strength of frictional weakening relative to the inertial and elastic properties of individual blocks and $v_c = {1}/{b_f \omega D}$. In this paper, we focus on how the prestress and slips responds to different stiffness ratio, r and the rate weakening parameter, v_c.

The modified spring block model can be beneficial and insightful for different reasons. Firstly, taking off the loading plate and apply the pulling force only at the edge block would simulate the cases that fracture occurs directionally. In other words, the rupture initiates at a given location and dissipate stresses down to the rest of the locations. Secondly, this modified spring block model reduces heterogeneity involved by complex stress stored in leaf springs to some extent, which can be informative for studying general chaotic behavior and self-organization of the one dimensional fractural system.

CHAPTER 3

PARAMETRIC SIMULATION RESULTS

Long-term parametric studies have been done to investigate the statistical properties of stress and slip in spring block model. In particular, we are interested in how the patterns of event size, pulling force and average rupture stress could change with the two constitutive parameters: 1. the stiffness ratio, r, between the first pulling spring and the coil spring connected each block; 2. velocity-weakening coefficient, v_c, which measures how friction is weakened as slip rate increases. In the following sections, we use a chain of 1000 blocks, n=1000 and test the system for about 100000 events for each case.

3.1 Effects of model parameters on event sizes

In this section, we explore the effect of parameters on the size distribution of events generated in our simulations. The spring stiffness ratio, *r*, is the ratio of the spring stiffness that interconnect all the blocks (k_c) to the spring stiffness connected to the pulling force (k_l). The velocity weakening coefficient, v_c, gives a measure of frictional weakening. Event size is defined as how many blocks have been moved during one single event. Initially, a pulling spring is connected to the first block and applying a pulling stress to the first block. Once the pulling force exceeds the static friction of the first block, the first block moves. The slip of the first block will transfer stress to the next spring block and may or may not cause the slip to the other blocks, which depends on the stiffness of the spring and friction. An event ends when all the blocks stop moving. In Figure 2, the slip profile across the spring block is presented for a large event and a medium event. A large event indicates that all the blocks have undergone displacement in a single event. And a medium event means that nearly half of the blocks move during an event. In this section,

we investigate a parametric study to illustrate how stiffness ratio, r and velocity-weakening coefficient, v_c, affect event size distribution.

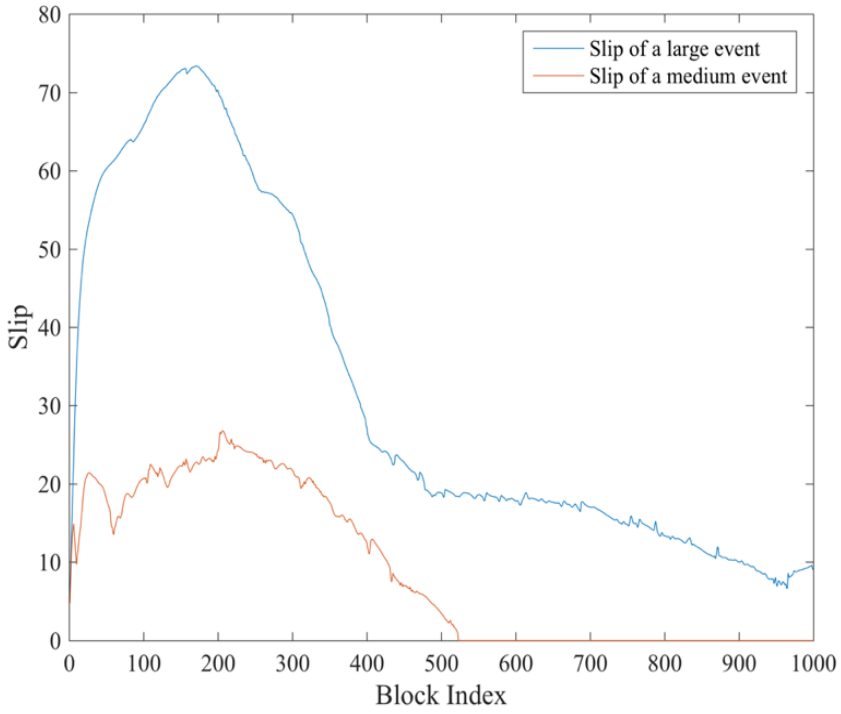

Figure 2: Slip profile of a system of blocks undergoes a large event and a medium event.

3.1.1 Effects of stiffness ratio

Stiffness ratio r is the ratio between spring stiffness of inner spring and the pulling spring. $r = {k_c}/{k_l}$. A small value of r indicates weak springs connected to the block system while a large value of r indicates stiff springs between all the blocks. Theoretically, r could range from zero to infinity. An infinity r reveals that the system of spring block model is a rigid bar and all the block can be regarded as an unity. Thus, for large value of r, we expect the more blocks to slip, which gives large events. In the case of zero stiffness ratio, the springs interconnected all the blocks are extremely weak which suggests that all the blocks are independent to each other. Therefore, for

small r, we expect mostly small sized events. Figure 3 and 4 present the distribution of event length for different value of stiffness ratio while keeping frictional weakening as constant. In Figure 3, there is an apparent increase in event complexity and size distribution as stiffness ratio increases. It should be noted that when r is 0.01, there are large events happened. However, for each case, the system runs for about 0.1 million events. Despite these large events, all the rest of the events have a small event size less than 10. The presence of large events in this case is a combined result of frictional weakening and stiffness ratio. As r increased to 0.1, there is an obvious trend of built up small events before several large events. For the case r is 1, the increase of spring stiffness results in more and larger events.

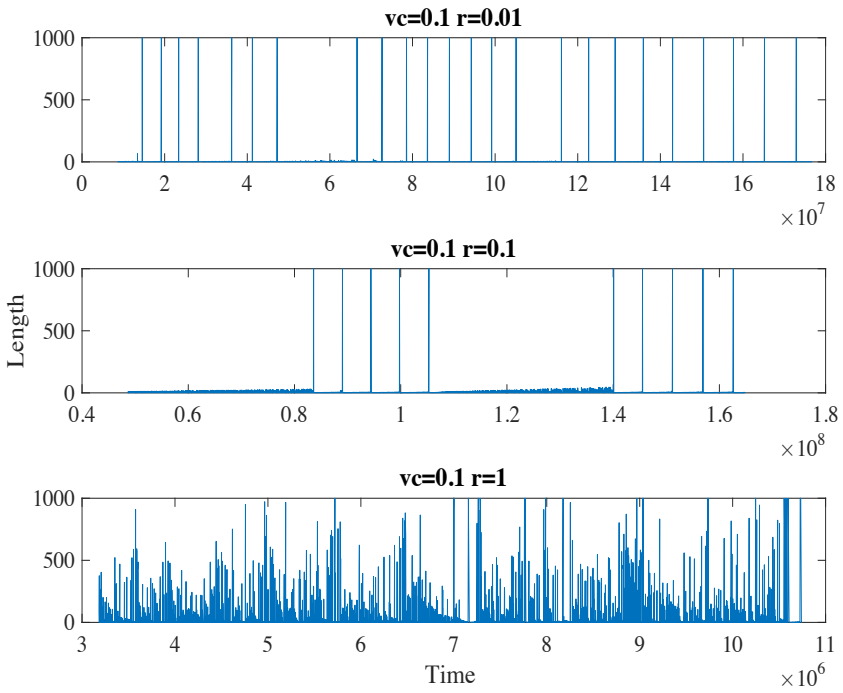

Figure 3: Distributions of event size with velocity-weakening parameter, v_c equals to 0.1 and stiffness ration r varying from 0.01 to 1, in which r=0.01, 0.1 and 1 corresponds for weak springs, medium springs and stiff springs. Note that stiff springs generate large and complex events distribution whereas weak springs only lead to several full-length fractures.

In Figure 4, as the velocity weakening coefficient v_c is held at 0.5, the general size distribution is dominated by small events. As the stiffness ratio r is increased from 0.01 to 1 there is an increase in the number of medium events generated by larger r value. It should also be noted that the time for each case of r to reach 0.1 million events are different. For r=0.01, the time required for the system to complete 100,000 event cycles is about 4*10^7, while for r=1, the time is shortened to 7*10^6. The stiff springs cause the evolvement of fracture to happen faster since each block is more dependent.

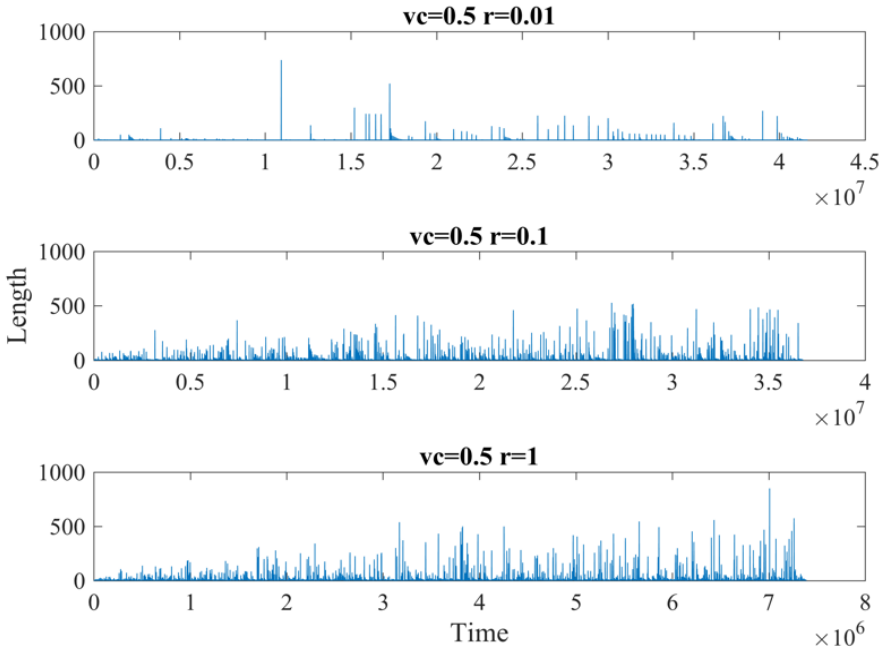

Figure 4: Distributions of event size with velocity-weakening parameter, v_c equals to 0.5 and stiffness ration r varying from 0.01 to 1, in which r=0.01, 0.1 and 1 corresponds for weak springs, medium springs and stiff springs. Note that stiff springs generate denser event size distribution and weak springs only generate small sparse events.

3.1.2 Effects of velocity weakening coefficient

From Equation 2.7, the friction term in the equation of motion for each block is correlated to the velocity weakening coefficient, v_c. The dissipative frictional force is defined as $\frac{1}{1+\frac{\dot{U}_i}{v_c}}$.

Thus, frictional weakening is enhanced by small value of v_c. In this section, a strong rate-weakening friction corresponds to a fast drop of friction as slip rate increases. A small value of v_c reflects to a strong rate-weakening friction law and a large value of v_c indicates a weak rate-weakening friction law. In this study, we observe that in general, a strong rate-weakening law leads to more and larger events since the energy dissipate on friction is relatively small. The system evolves to larger events. In Figure 5, it is not obvious how rate weakening affects the size distribution, as vc changes from 0.01 to 0.1. This is because at this point, the effect of stiffness ratio dominates since the system is stiff. Comparing to Figure 6, where r is 0.1, as vc changes to 0.16 to 0.08, there is an obvious tendency of increase in event size. In this case, the effect of friction weakening dominate. For both case, when vc is higher than 0.5, we observe that a weak rate-weakening law only generate small events.

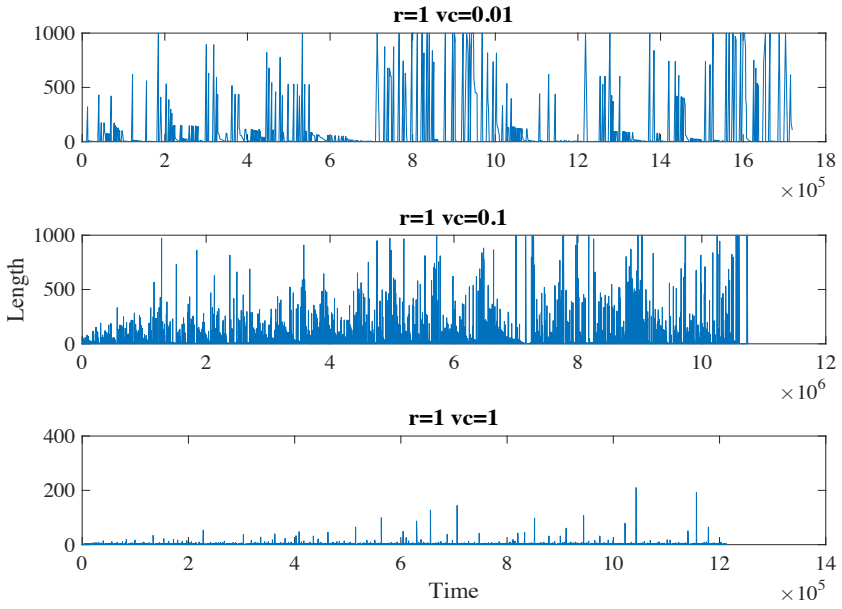

Figure 5: Distributions of event size with stiffness ration, r equals to 1 and varying velocity-weakening parameter, v_c, from 0.01, 0.1 to 1. In the case when v_c=0.01, friction is greatly reduced by velocity and energy dissipated in friction is relatively small, causing large event dominated size distribution. In the case when v_c=0.1, velocity-weakening strength is moderate. The event size distribution is dominated by medium events. In the case when v_c=1, friction is decreased slightly by velocity, kinetic energy is dissipated by friction and only small-scale ruptures occur.

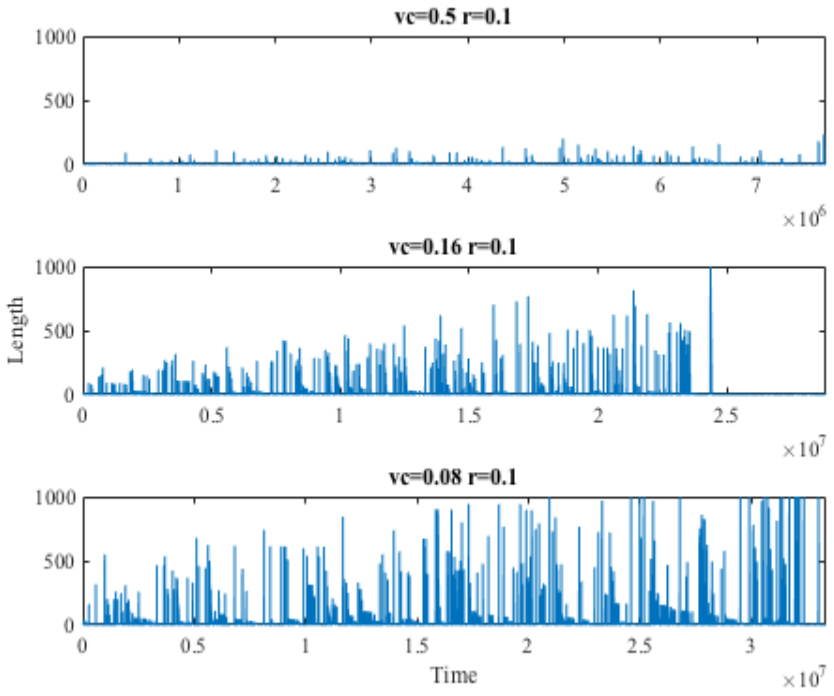

Figure 6: Distributions of event size with stiffness ration, r equals to 0.1, and varying velocity-weakening parameter, v_c, from 0.5, 0.16 to 0.08. In the case when v_c=0.08, friction is greatly reduced by velocity and energy dissipated in friction is relatively small, causing large event dominated size distribution. In the case when v_c=0.16, velocity-weakening strength is moderate. The event size distribution is dominated by medium events. In the case when v_c=0.5, only small-scale ruptures occur.

In order to study the impact of velocity weakening to size distribution, we generate Figures 7 and 8 with x-axis of log of event length and y-axis of log of number of event with the same event length. In Figure 7, as r is 0.1, in all cases, the curve log number of events versus log length correlates to v_c value. Stronger velocity weakening generates more events since the curve of smaller v_c is above curves with higher v_c. A power law could be deduced when v_c is less than 0.32 for length is less $10^{1.7}$. This can be useful to estimate event number with a specific size. It is also worth noting that strong velocity-weakening friction law corresponds to this relation. In Figure 8, r is 10 with different v_c value. In this case, the stiffness ratio is 10 and thus, the size distribution is dominated by r. This explains why the shape of curves are not similar to what is shown in Figure

7. However, the same power law between number of events and length is found for strong rate-weakening law, vc smaller than 0.32 with length less than $10^{1.5}$. This relation is beneficial for estimating and predicting the number of events with a specific rupture length.

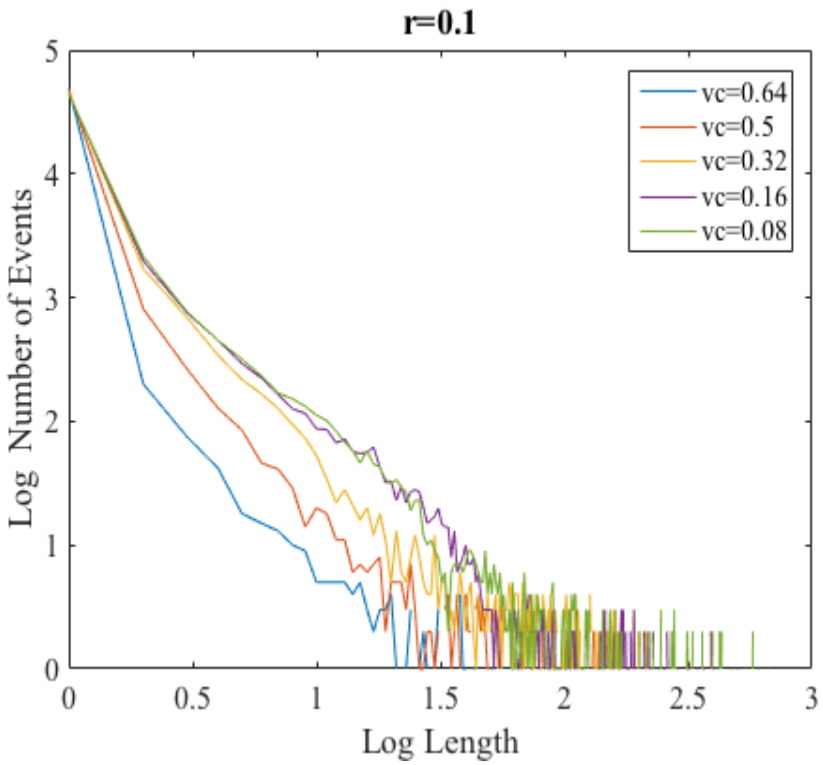

Figure 7: Distribution of event size for different v_c when r=0.1. The horizontal axis is log of event length. Since the system is 1000 blocks, the maximum length of the event is 10^3. The vertical axis is number of events with the corresponding size of event. For instance, when log length is 0, (length=1), the corresponding number of events is about $10^{4.7}$. Note that in this figure, the number of events with size is 1 is not identical. The curves do not intersect at log length=0.

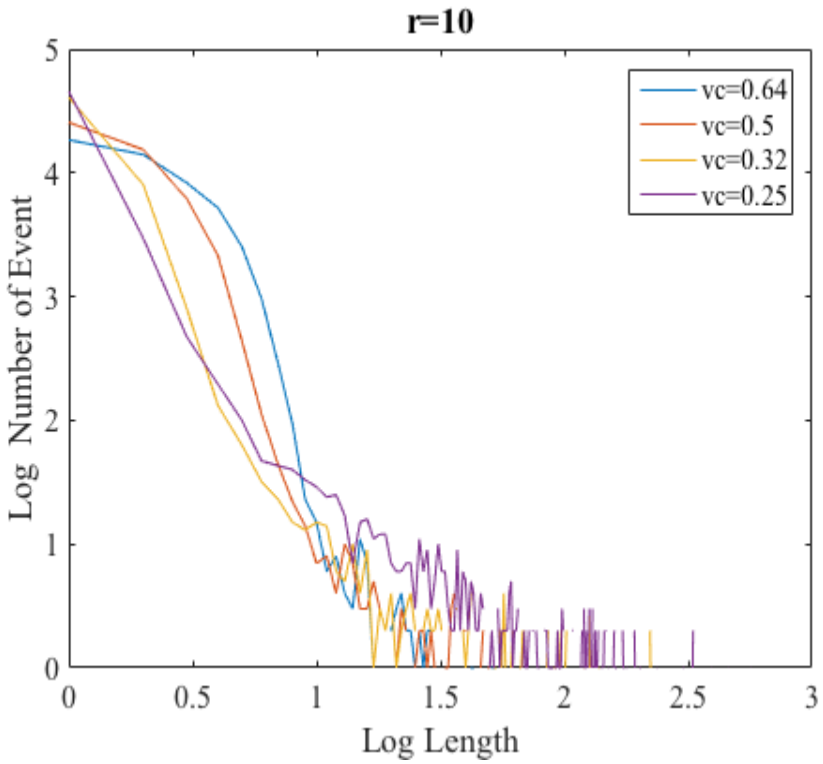

Figure 8: Distribution of event size for different vc when r=10. It can be observed that a nearly power law for number of event and length could be found for vc is less than 0.32.

Figure 7 and 8 indicate the relationship between the number of events and event size for small events (typically less than 50). In Figure 9, it is observed that this relation also exists for large and medium events. The horizontal axis is event size, and the vertical axis is cumulative number of events corresponding to equal or higher event length. The slope of the curves changes with vc. This relation could be used to estimate the total number of event larger than a specific event length for different values of vc.

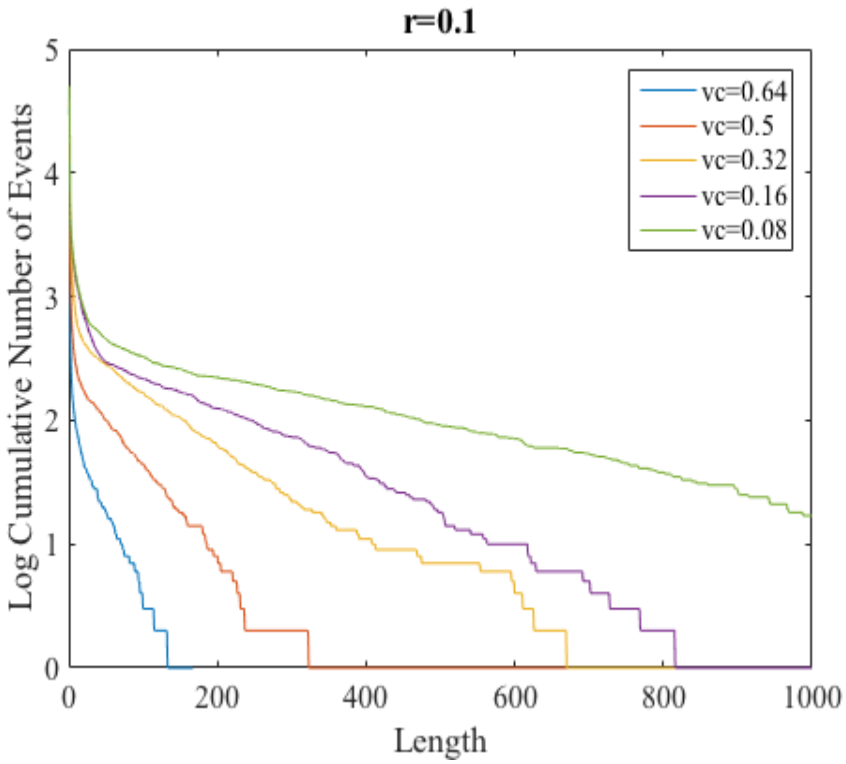

Figure 9: The event size distribution for r=0.1 and various v_c. The horizontal axis is event length. The vertical axis is cumulative number of event with equal or larger event length. Note that the plot starts with length=50. This is because in figure 8, the power law is found for event length is less than $10^{1.7}$.

3.2 Effects of model parameters on pulling force

Pulling force is the force subject to the pulling spring which connect to the first block and with a constant loading rate, v_p. It is the external force applied to the spring block slider model to cause dynamic rupture. By comparing the length distribution with pulling stress distribution for the same parameter, we can see that for each large event, there is a drop of pulling stress. As shown in figure 10 when vc=0.1 and r=0.1, the pulling force is built up and reach the peak where a full fracture occurs. The pulling stress drops after a large event and continues to build up until another large event happens. This observation also applies to other combination of vc and r.

In Figure 10, when vc is 0.1 and varying r from 0.1 to 0.0001, the magnitude of pulling stress decreases with small r. In the case of vc=0.1 and r=0.0001, the pulling stress is almost

constant. The negative value of pulling force is due to the displacement of the first block passing the displacement of the pulling spring. Thus, the pulling spring is in compressive stress. In Figure 11, vc is held at 0.5 and r varies from 1 to 0.01. The magnitude of pulling stress is enhanced by smaller value of r. In the case where vc is 0.5, the pulling force is continuously building up for all the values of r. Since the frictional weakening is low, energy dissipated in frictional force resists the block chain from undergoing large slip. Therefore, the pulling stress is always positive and with a general trend of increasing.

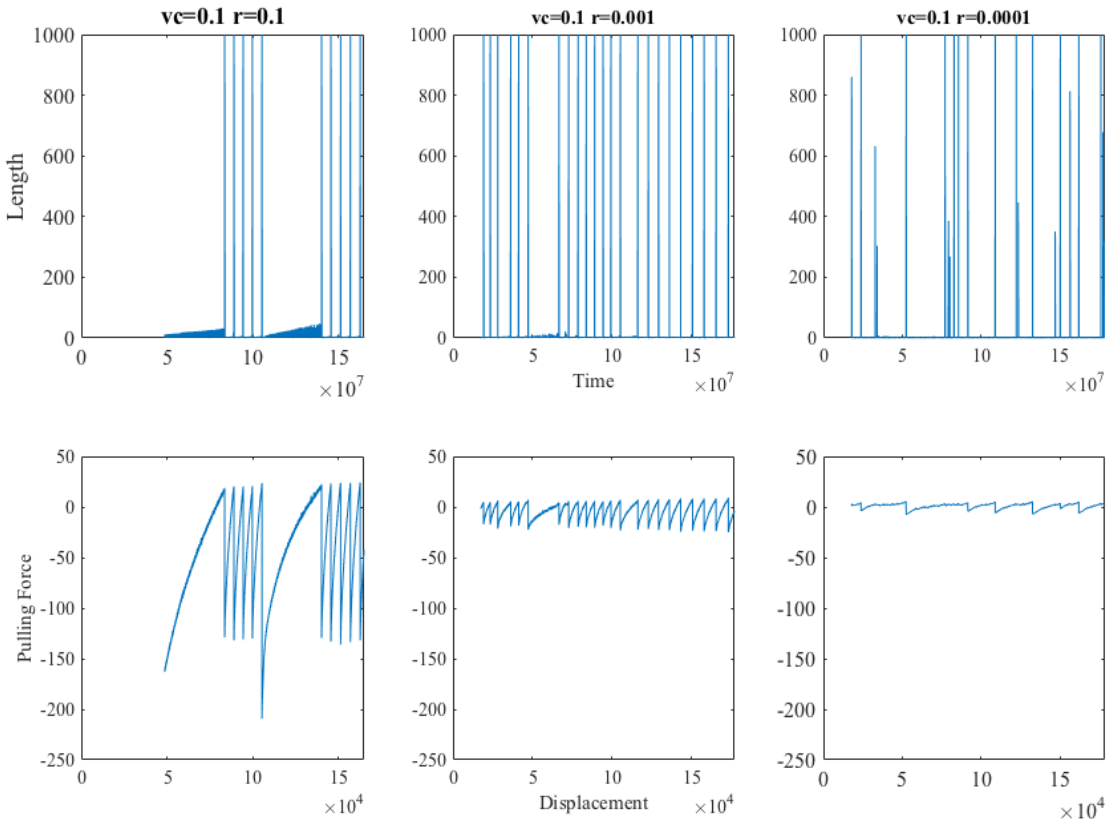

Figure 10: Comparison of pulling stress versus displacement with v_c=0.1 and r is 0.1, 0.001 and 0.0001 respectively. The upper plots are the event length distribution with horizontal axis of time and vertical axis of event length. The lower layer of plots is the pulling force versus displacement of the pulling spring with the corresponding v_c and r value. Note that the pulling spring is subject to a constant pulling velocity, $v_{p,}$ which is 10^{-3}. The negative pulling force indicates a compressive stress.

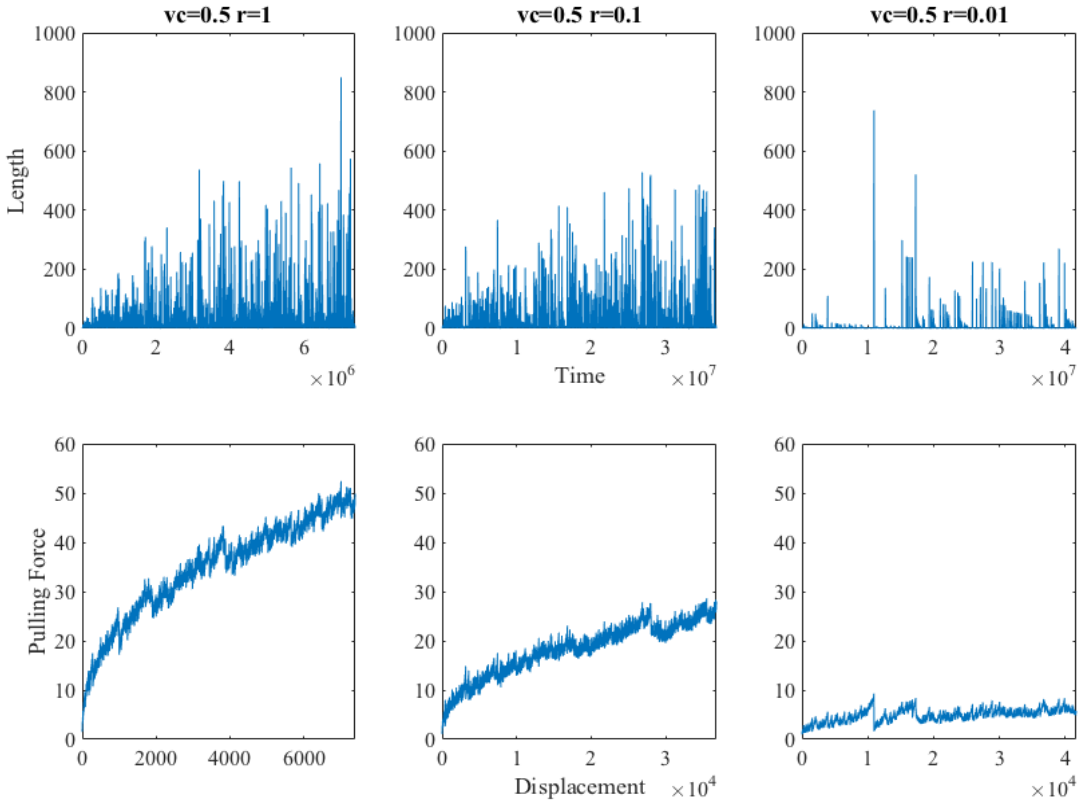

Figure 11: Comparison of pulling force versus displacement with v_c=0.5 and r is 1, 0.1 and 0.01 respectively. The upper plots are the event length distribution. The lower layer of plots is the pulling force versus displacement of the pulling spring.

Figure 12 shows that for vc=0.1, how the pulling force changes with stiffness ratio varying from 0.1 to 0.001. For r=0.001, the system is extremely ductile which is reflected by the fact that each of the blocks are nearly independent to each other. In this case, the external force applied to this system to generate a new rupture is nearly a constant, which could be regarded as creep fracture. For r=0.1, although the stiffness ratio is still small, the variation of external pulling force is relatively large. In this case, the external pulling force alternate and generate cyclic stress to cause fracture of a stiffer system. This is noted as fatigue fracture.

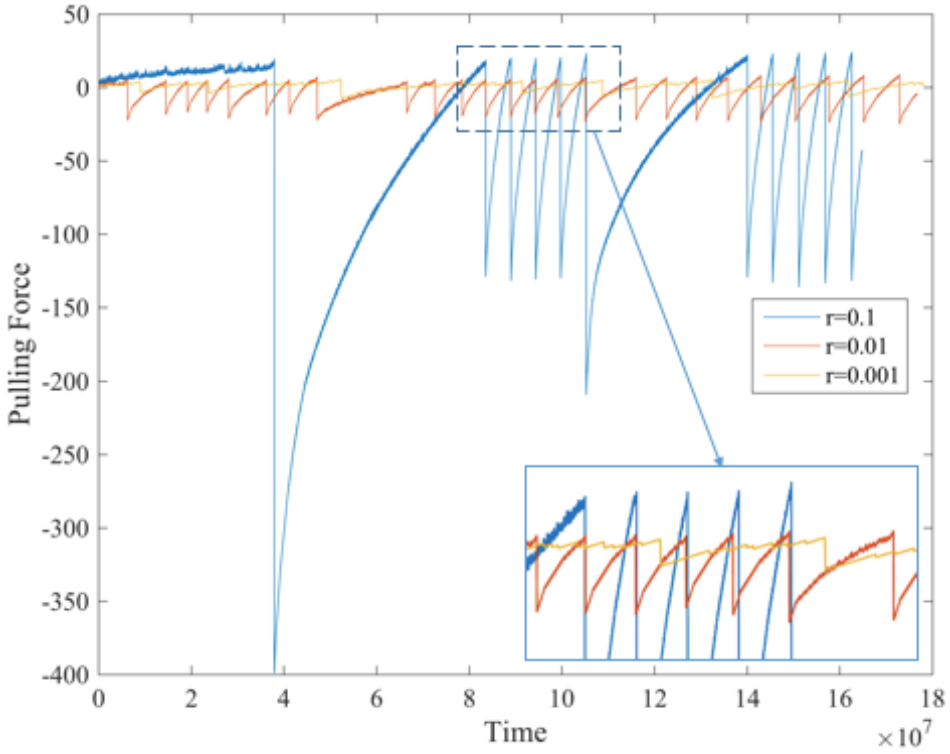

Figure 12: Comparison of pulling force with r equals to 0.1, 0.01 and 0.001 where v_c=0.1.

3.3 The relations between average rupture stress and event length

The average rupture stress of a single event is the average of stress over the rupture area, blocks that have slipped in that particular event. It is computed as the sum of stresses of those blocks that displaced during an event divided by the length of this event. An example of stress distribution before an event is illustrated in Figure 13. The average rupture stress is differed from mean stress since a block may not sip but the magnitude of stress at this block is nonzero.

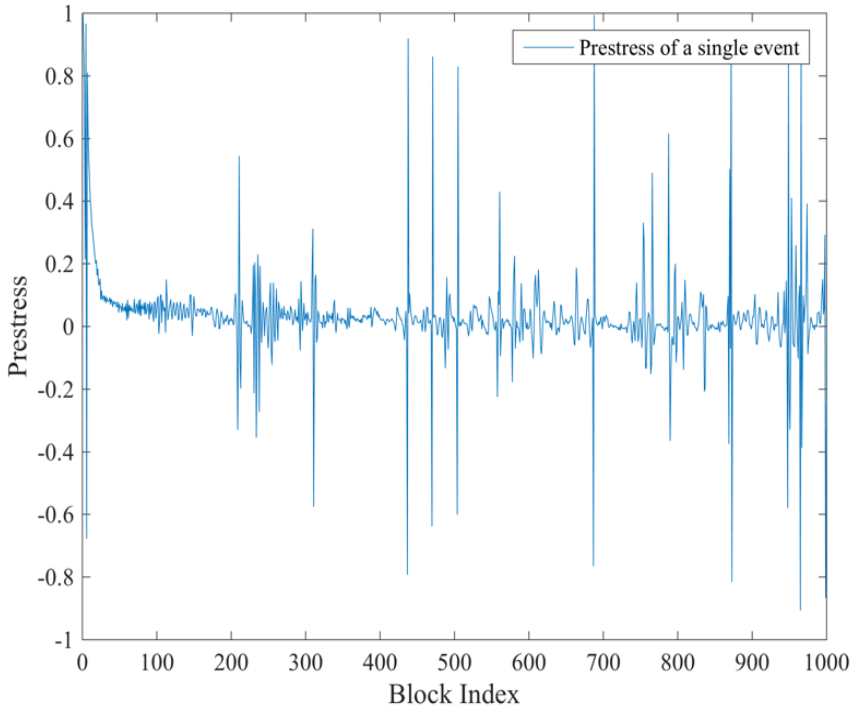

Figure 13: Example of prestress distribution exists in the system.

After a series of parametric studies, we found a power law relation between average rupture stress and event length, as shown in Figures 14 to 17. As the length of event increases, which indicates a large event, the average rupture stress at this particular event decreases. An empirical equation between average rupture stress and event length can be generalized from these figures. We set σ as average rupture stress, L as event length, k is the slope of the fitted linear relation for log σ, and log L and c is the intercept of the fitted line on the y-axis. A relation of log σ = klog L + c could capture how average rupture stress diminished with event length. Specifically, in this section, we are interested to investigate how the parameters r, and v_c influence the rate of mean rupture stress decrease with length, the slope of the fitting line.

In Figure 14 to 17, it is obvious to notice that the magnitude of slope increases with smaller stiffness ratio. Figure 14 to 17 compare log average rupture stress versus log event length for a constant v_c and different r value. As the block system become softener, the average rupture stress to generate a particular event size is reduced. However, the effect of frictional weakening to the magnitude of slop is vague. In Figure 14 and 15, both of the plots with r varying from 1, 0.1 and 0.01, the magnitude of slope for v_c=0.5 is -0.45, -0.55 and -0.75; whereas the magnitude of slope for v_c=0.1 is -0.5, -0.8 and -0.9. By comparing these two cases, strong velocity weakening may result on higher magnitude of slope. However, when comparing the case (v_c=1, r=0.1, k=-0.55) in figure 16 with (v_c=0.5, r=0.1, k=-0.55) in Figure 14, this relation of v_c to slop does not hold. The rule does not hold neither for comparing the case (v_c=0.05, r=0.1, k=-0.7) in Figure 17 with (v_c=0.1, r=0.1, k=-0.8) in Figure 15 or comparing the case (v_c=0.05, r=0.01, k=-0.85) in Figure 17 with (v_c=0.1, r=0.01, k=-0.9) in Figure 15. Although the effect of v_c to how fast average rupture stress changes with length is not clear at this point, it is worth to note that for large v_c, weak frictional-weakening, the mean rupture stress nearly does not drop with length for small event. In Figure 16, for log length less than 1.5, the mean rupture stresses near not vary with length.

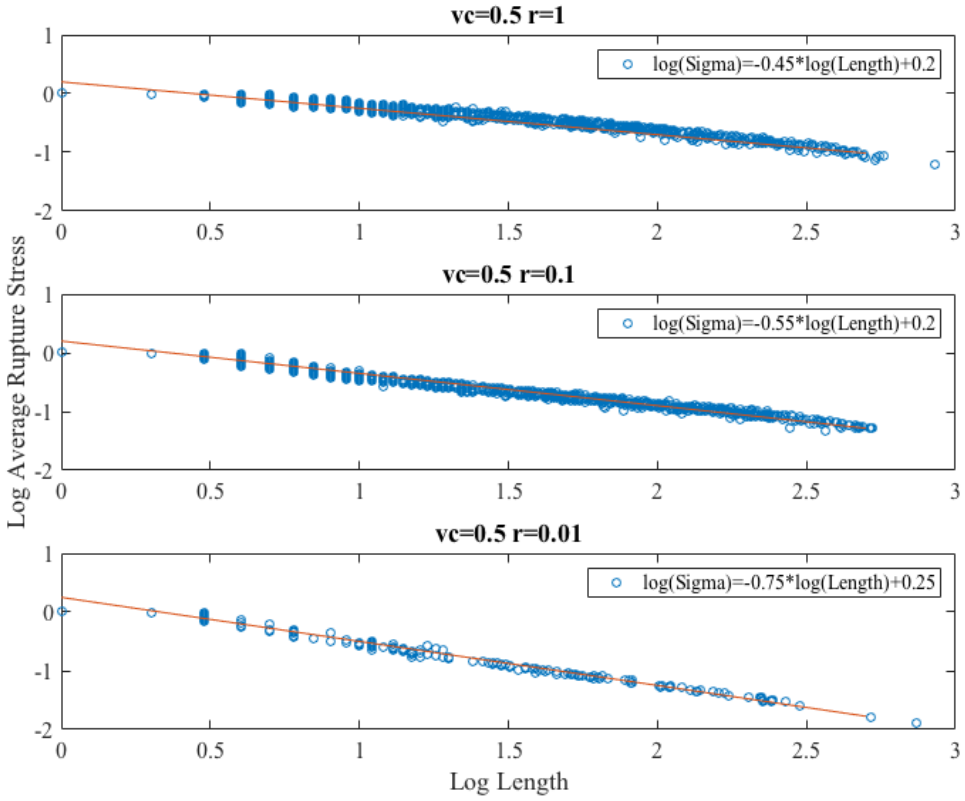

Figure 14: Log average rupture stress versus log event length for v_c=0.5 and varying r from 1, 0.1 and 0.01. The horizontal axis is log of event length and vertical axis is log of average rupture stress. The blue circle indicates that at a particular event, the corresponding mean rupture stress with length of that event. The red line is a fitting line for this power law relation. Note that the magnitude of slop increases as r drops.

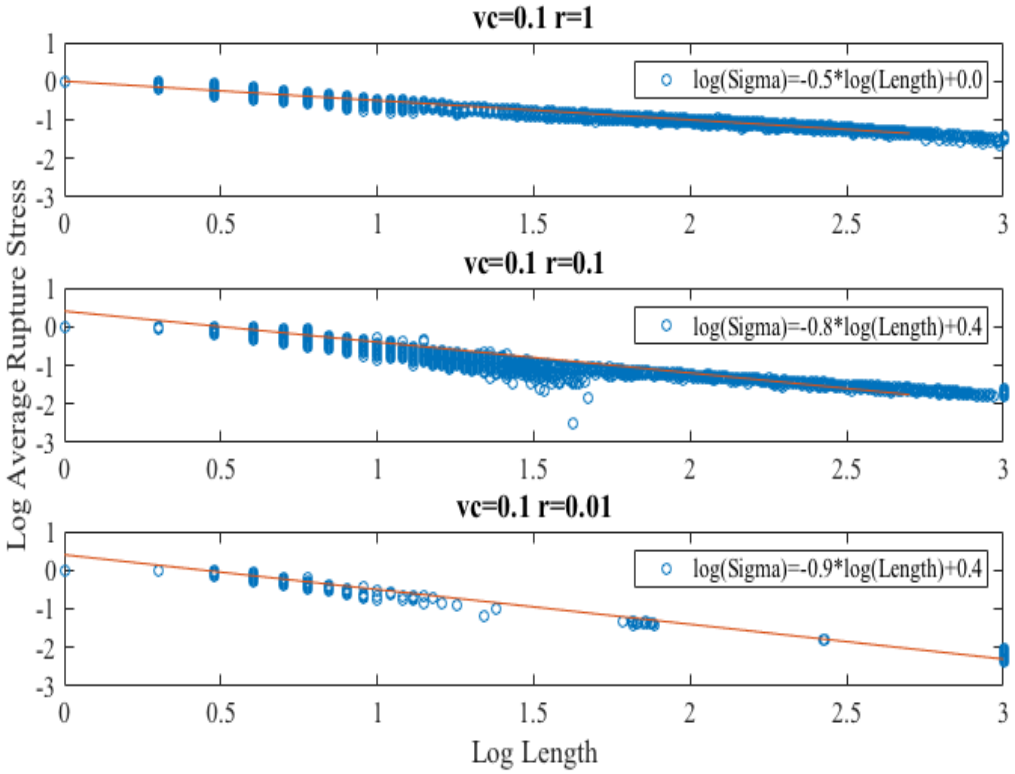

Figure 15: Log average rupture stress versus log event length for v_c=0.1 and varying r from 1, 0.1 and 0.01. Note that the magnitude of slop increases as r drops.

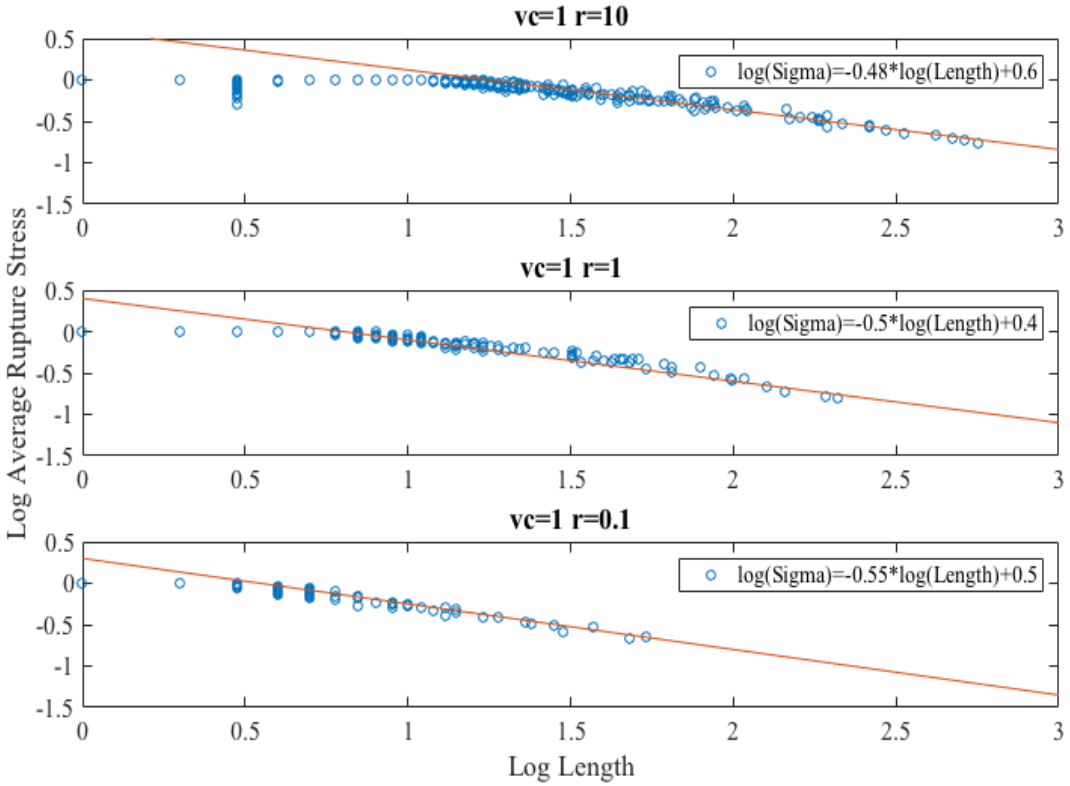

Figure 16: Log average rupture stress versus log event length for v_c=1 and varying r from 10, 1 and 0.1. Since the friction weakening coefficient v_c is large, the effect of mean rupture stress drops with length for small event is negligible. Note that the fitting line only fit for events with size larger than $10^{1.5}$.

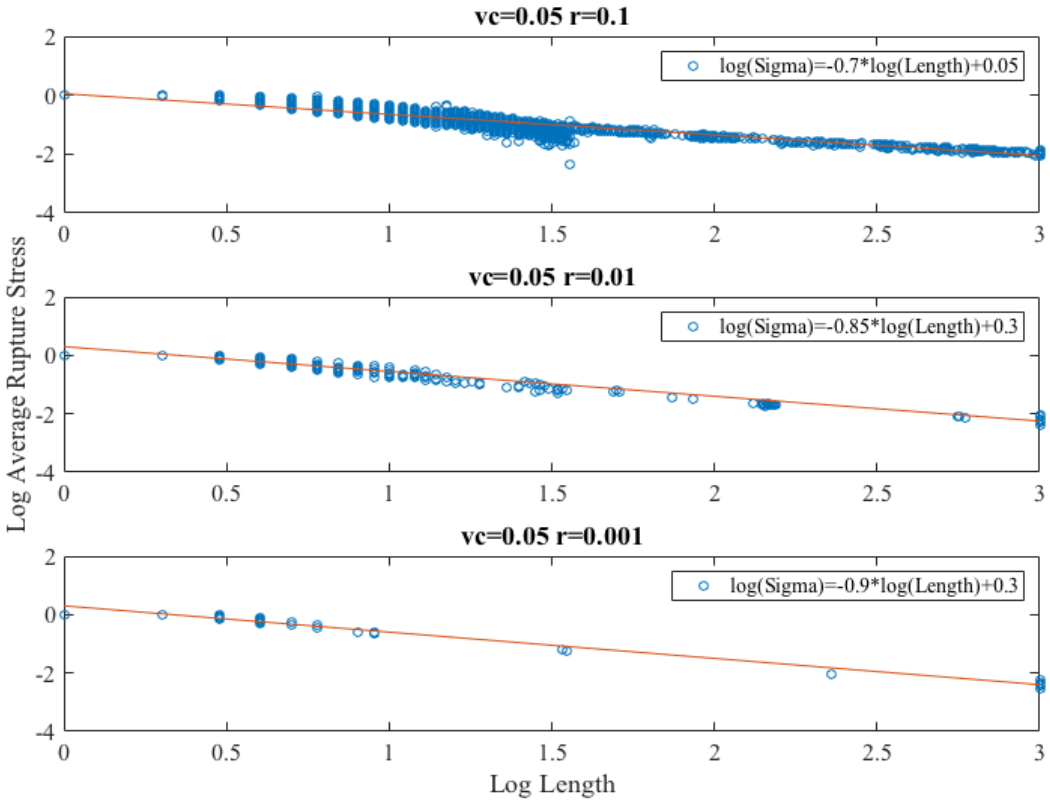

Figure 17: Log average rupture stress versus log event length for v_c=0.05 and varying r from 0.1, 0.01 and 0.001.

CHAPTER 4

APPLICATION: WATER INJECTION INDUCED SEISMICITY

4.1 Introduction and Project Overview

Man-made seismicity refers to typically minor earthquakes and tremors that are caused by human activity that alters the stresses and strains in the Earth's crust. Most induced seismicity is of a low magnitude. There are many ways in which induced seismicity has been seen to occur. In the past several years, some energy technologies that inject or extract fluid from the earth, such as oil and gas extraction and geothermal energy development, have been found or suspected to cause seismic events. [Hough, 2015] For example, wastewater from oil and gas production and carbon dioxide from a variety of industrial processes may be managed through underground injection.

In wastewater disposal, treated wastewater is injected into the ground between impermeable layers of rocks to avoid polluting fresh water supplies or adversely affecting quality of receiving waters. Injection wells are usually constructed of solid walled pipe to a deep elevation in order to prevent injection from mixing with the surrounding environment. [EPA, 2015] An injection well is a device that places fluid deep underground into porous rock formations, such as sandstone or limestone, or into or below the shallow soil layer. The fluid may be water, wastewater, brine (salt water), or water mixed with chemicals. Injection wells are widely considered to be the best method for disposal of treated wastewater.

4.2 Model Setup and Pore Water Pressure Reduction Factor

The setup of the spring block slider experiment is shown in Figure 18. The model used for the simulation of fault slip consists of a chain of N blocks with identical mass (m). Each of the blocks is connected by coil springs with stiffness (k_c) to its neighboring blocks' and each of them

is connected by a moving plate with leaf springs, (k_l). The moving plate is subjected with an initial velocity (v_p). Once the pulling force exceeds static friction, the block will move. It will further transfer stresses to its neighboring blocks and causing them to move if the elastic force exceeds static friction. A dynamic friction force ϕ is used to represent the friction between blocks and the surface when the blocks are moving. An event is complete when all the blocks stop sliding.

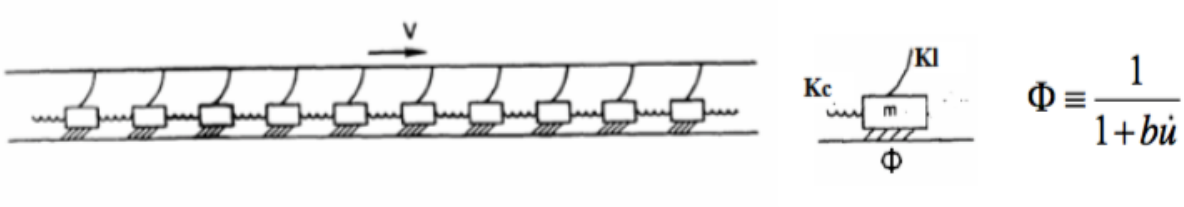

Figure 18: One-dimensional spring-block-slider model

Once the static friction is exceeded, the motion of the i^{th} block (u_i) is given by the following differential equation:

$$F = m\ddot{u}$$

$$m_i\ddot{u}_i = k_c(u_{i+1} - 2u_i + u_{i-1}) + Kl(v_P t - u_I) - F_{st}\frac{1}{1+b_f\dot{u}_i} + \sigma_{oi} \quad (4.1)$$

Equation (3.2.1) represents a set of n ordinary differential equations where n is the number of blocks; each of these ODE's are nonlinear because of the friction term. We use a second order predictor-corrector scheme for solving Equation. (4.1). The material and frictional properties are assumed to be spatially homogeneous. [Elbanna, 2011]. The time step is controlled by the ratio of the spring stiffness connected to the pulling force to coil spring stiffness, $r = k_l/k_c$ and the rate

of frictional weakening, b_f [Elbanna, 2011]. We assume uniform masses, m =1, and local static frictional strength, F_{st} = 50. We rewrite Equation (4.2) in the following form:

$$\ddot{u}_i = r(u_{i+1} - 2u_i + u_{i-1}) - u_i - \frac{c(i)}{1+\dot{u}_i \backslash vc} + \sigma_{oi}/F_{st} \tag{4.2}$$

Where $r = k_l/k_c$, representing the stiffness ratio. The ratio v_c measures the strength of frictional weakening relative to the inertial and elastic properties of individual blocks. In this paper, we focus on how the prestress responds to different stiffness ratio, r and the rate weakening parameter, v_c. c(i) is a reduction of normal force due to the reduction of pore water pressure under the circumstance of water injection. c(i) is always less than one. The detailed description of c(i) will be presented in the next section.

4.2.1 Pore Water Pressure Reduction Factor

Case 1: Constant stress reduction

In this stress distribution, the normal stress in a specified area is reduced constantly as follows:

$$reduction\ factor = \begin{cases} 1 & (x < x_1) \\ r(<1) & (x_1 < x < x_2) \\ 1 & (x > x_2) \end{cases} \tag{4.3}$$

where x_1 and x_2 defines the area of stress reduction and r defines the ratio of stress reduction. This reduction factor is multiplied by the stress distribution without the crack to generate the stress distribution when there is the crack. The example of constant stress reduction is shown below. In this example, the reduction factor for $x_1 = 100$, $x_2 = 200$ and $r = 0.7$ is presented.

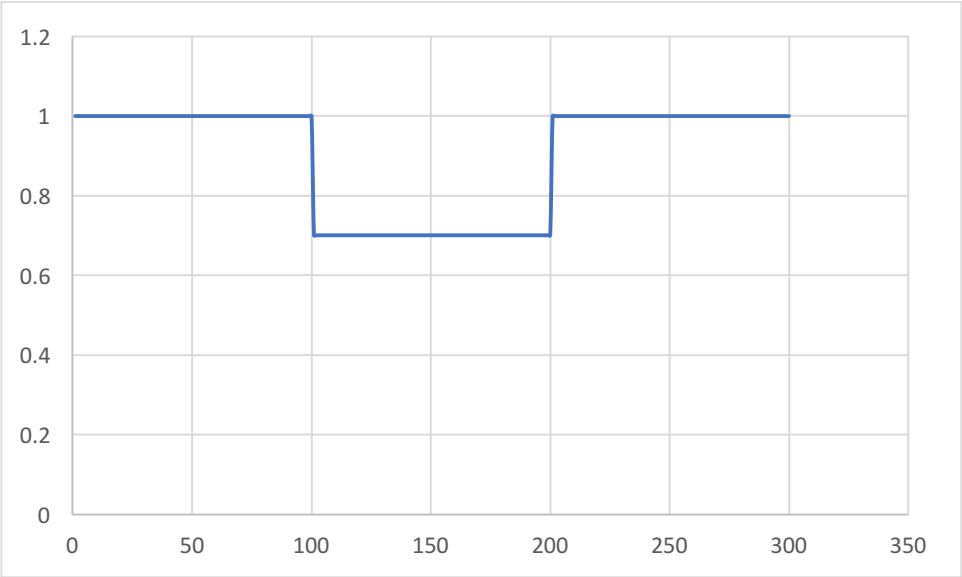

Figure 19: Constant stress reduction.

Case 2: Gaussian stress reduction

In this stress distribution, the normal stress around the crack is reduced according to Gaussian distribution as follows:

$$reduction\ factor = 1 - \frac{a}{\sqrt{2\pi\sigma^2}} \exp\left(-\frac{(x-\mu)^2}{2\sigma^2}\right) \tag{4.4}$$

Gaussian distribution can be defined by specifying the mean μ, the standard deviation σ and the constant amplification factor a of the distribution. The mean and the standard deviation of the stress reduction are set equal to the mean and the standard deviation of the uniform stress reduction in Case 1. The constant amplification factor is set so that the total stress reduction is equal to the total stress reduction in Case 1.

An example stress reduction factor corresponding to the example uniform reduction shown previously is illustrated below. In this example, the mean, the standard deviation and the constant amplification factor are 150, 28.9 and 30, respectively. These values are computed by the value of the parameters defined in the previous example of uniform stress reduction.

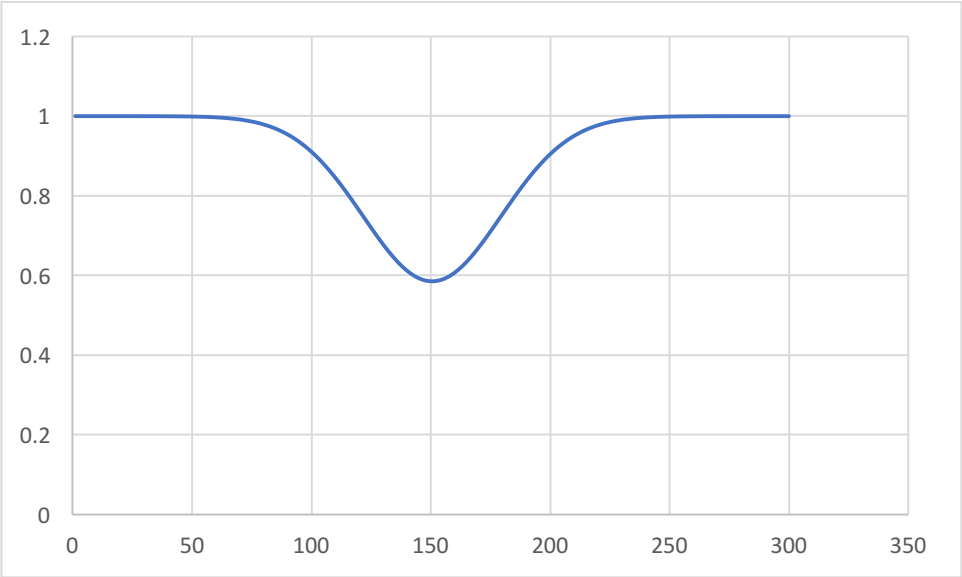

Figure 20: Gaussian stress reduction.

4.3 Results

4.3.1 Effects of Stress Reduction Factor on the Event Size

The model behavior is controlled by three main parameters: the stiffness ratio; and the strength of the velocity-weakening friction, and stress reduction factor c. In this section, we explore the effect of changing the value of stress reduction factor while the stiffness ratio and velocity-weakening level remains unchanged. For all the cases in this paper, the stiffness ratio is 0.1 and velocity-weakening level is 0.1. We use a chain of 1000 blocks, where n=1000 and maximum event number is 50,000. For the following three cases, we initiate water injection starting at event number 20,000 and ends at event 30,000. The blocks that allow stress reduction is from the 250^{th} block to the 500^{th} block. Figure 21 shows the event size distribution with no water injection. In other words, there is no stress reduction in the chain of blocks. Most of the events are small to medium event, with less than one half of the blocks have been moved. Figure

22 shows the event size distribution with stress reduction factor c=0.5. Average event size is about 400. There are more medium events. Figure 23 is the event size distribution with stress reduction factor c=0.3. The average event size is about 600. Comparing these three figures, it is clear that stress reduction and water injection would increase the event size. However, stress reduction does not bring extremely large events. It mainly adds on smaller events.

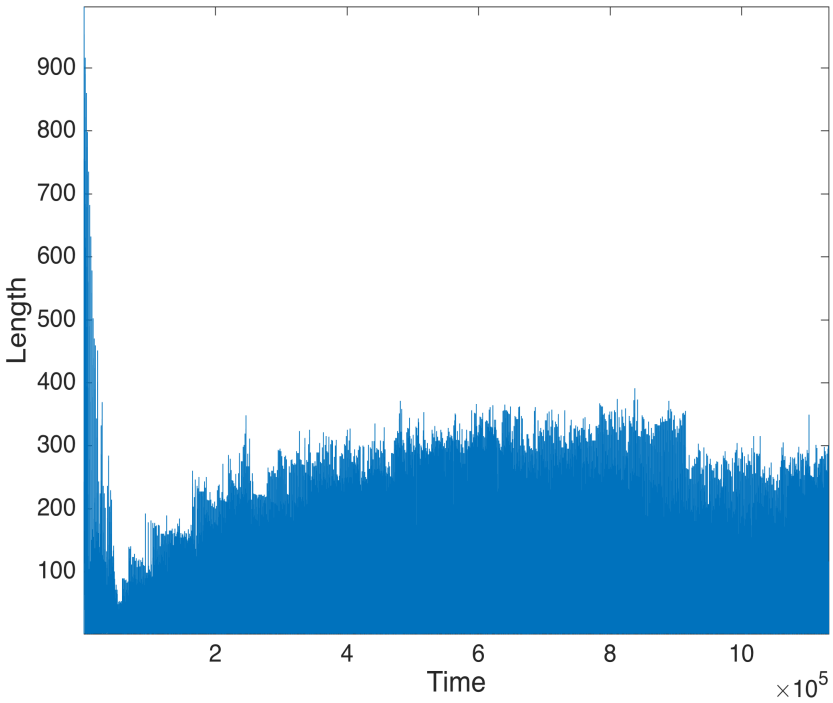

Figure 21: Event size distribution without water injection.

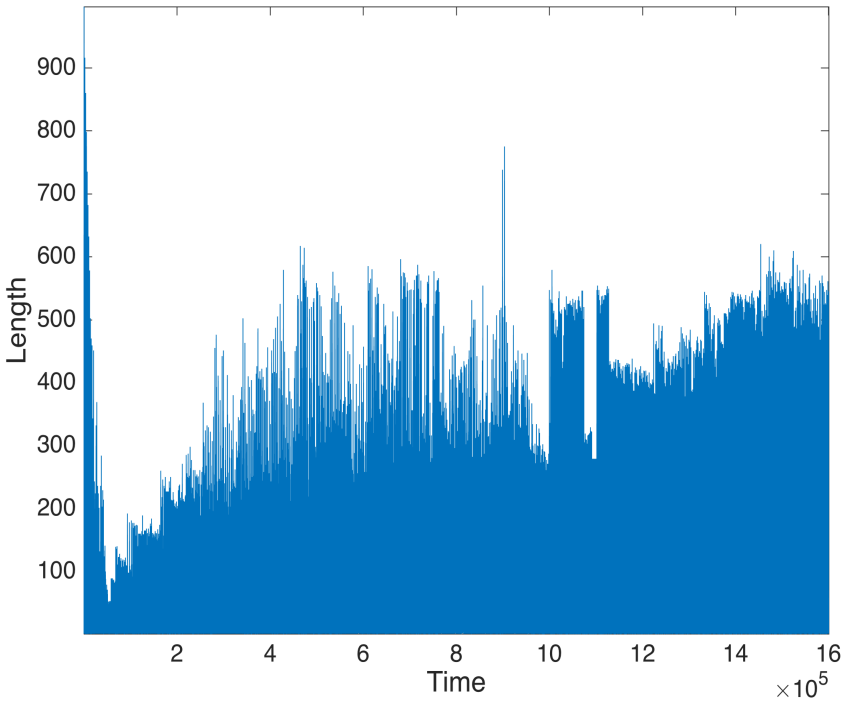

Figure 22: Event size distribution with medium stress reduction factor. c=0.5.

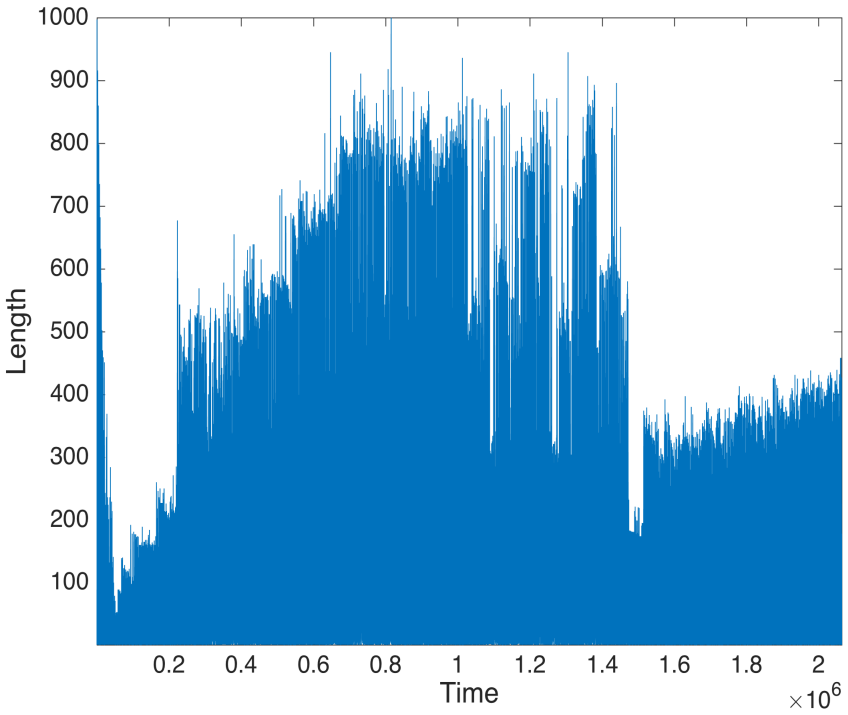

Figure 23: Event size distribution with high stress reduction factor. c=0.3.

4.3.2 Effects of Stress Reduction Factor on the average rupture stress

The average rupture stress is the mean of stresses over the length of an event. It is computed as the sum of stresses of those blocks that displaced during an event divided by the length of this event. After a series of parametric studies, we found average rupture stress has a tendency to decrease as the stress is reduced, as shown in Figures 24 to 26. Figure 24 shows the average rupture stress over length with no stress reduction. As the length of event increases, which indicates a large event, the average rupture stress at this particular event decreases. Figure 25 is the plot of average rupture stress versus length when there is a medium stress reduction, c=0.5. We can see clearly that the events rupture stress is shifted below of the one without stress reduction. For medium to large event, with length higher than three hundred blocks, there is a tendency that average rupture stress decrease as a reduction factor is subjected to the model. Figure 26 shows the average rupture stress for a high stress reduction factor when c= 0.3. There are two groups of events that the first group of events have their rupture stress reduced silently by event size. The second group events have their event rupture stress increased by event size.

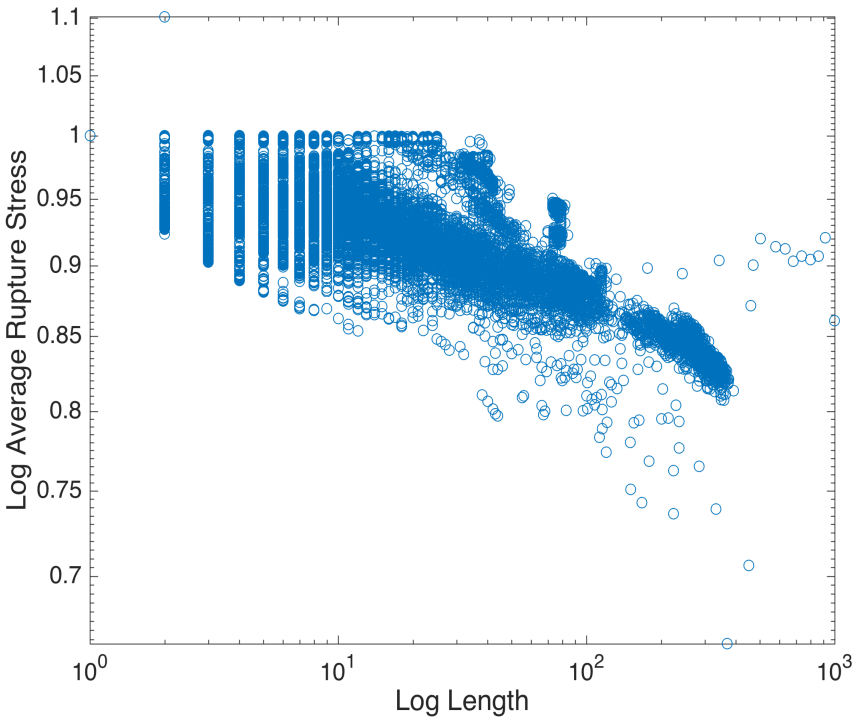

Figure 24: Average rupture stress vs event size for no water injection case.

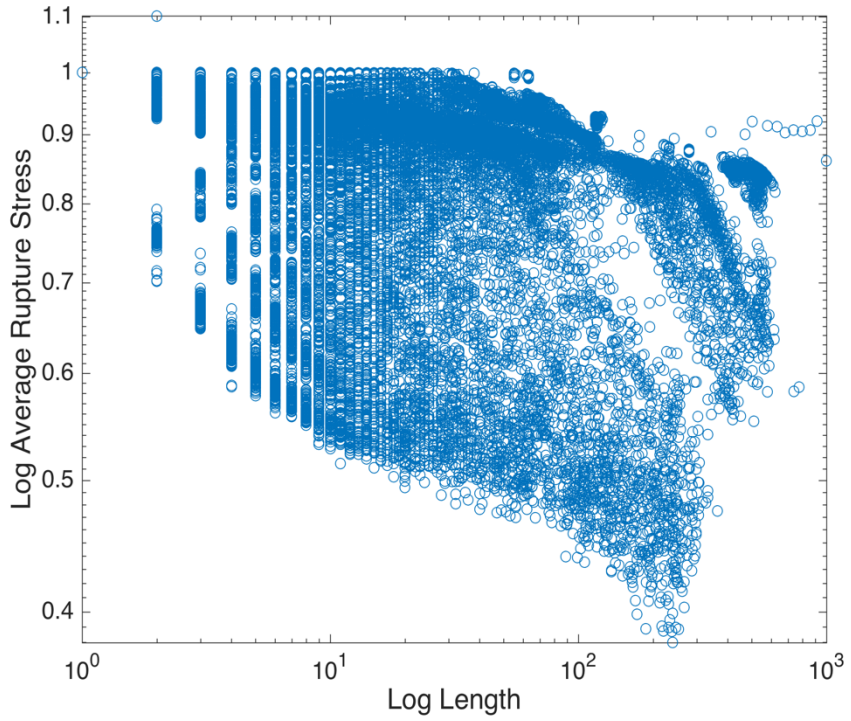

Figure 25: Average rupture stress vs event size for stress reduction=0.5.

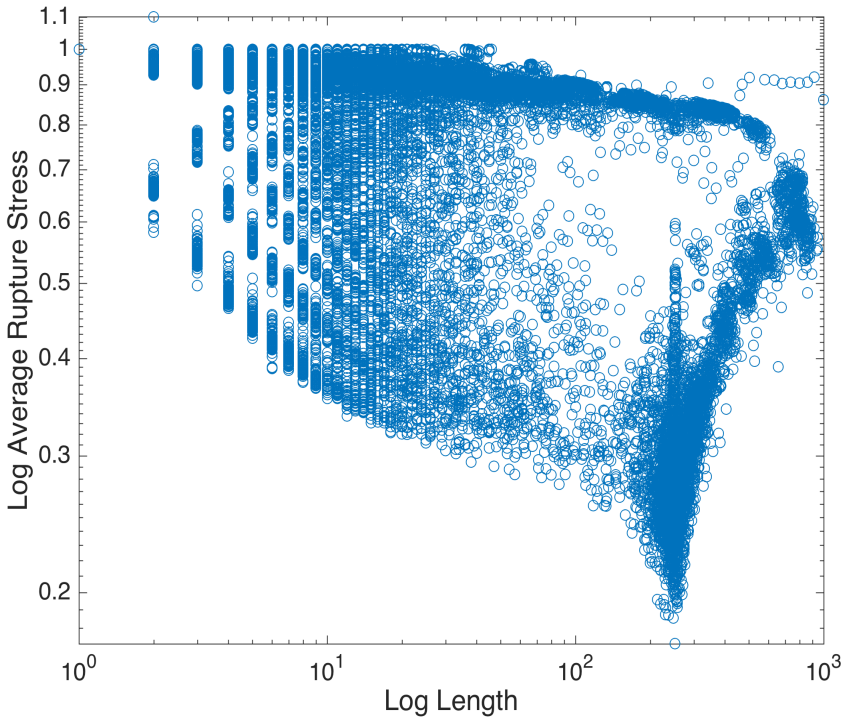

Figure 26: Average rupture stress vs event size for stress reduction=0.3.

4.4 Effects of water injection location on event size

In this section, we want to explore how the water injection location may impact earthquake mechanism. In the one-dimension spring block model, we have 1000 blocks interconnected. In the following cases, we change the location of stress reduction while keeping the reduction factor and injection time the same. For the following cases, we have c=0.5 and injection starts at the 20,000th event and stops at the 30,000th event. In Figure 27, 28 and 29, we have one quarter of the block chain subjected to a stress reduction, at the front quarter, the middle quarter and the end quarter of the block chain. We can see that the location of stress reduction will affect the size distribution. The event size for the stress reduction at end of the block chain is higher than the event size at the middle or at the front of the block chain. In Figure 30, we have the front half of the blocks being subjected to the stress reduction. The average event size is much higher than the previously cases

shown. This indicates that the more blocks being subjected to the stress reduction, the larger events are likely to happen.

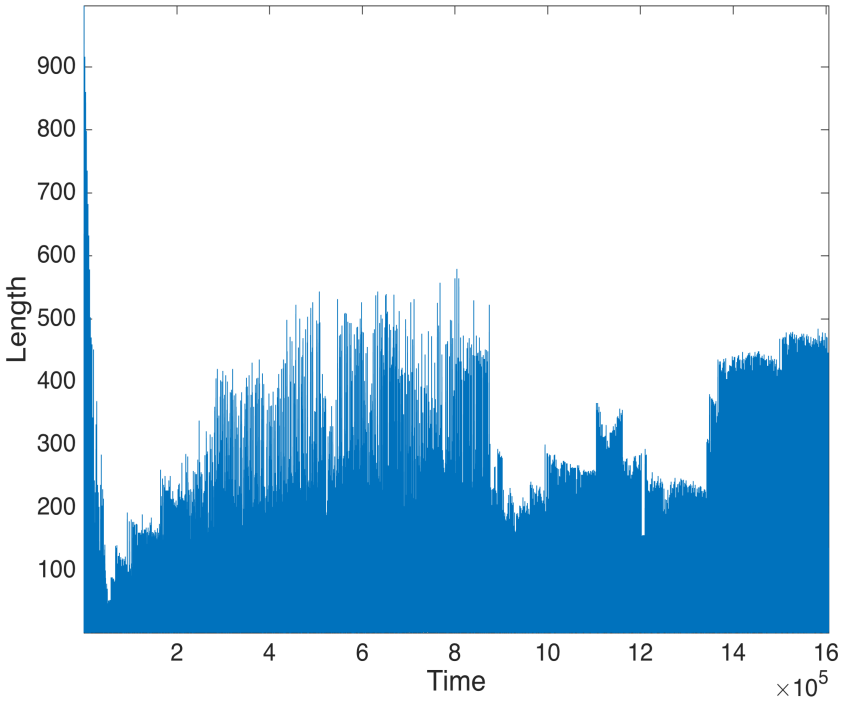

Figure 27: Event size distribution with water injection location at n=1:250.

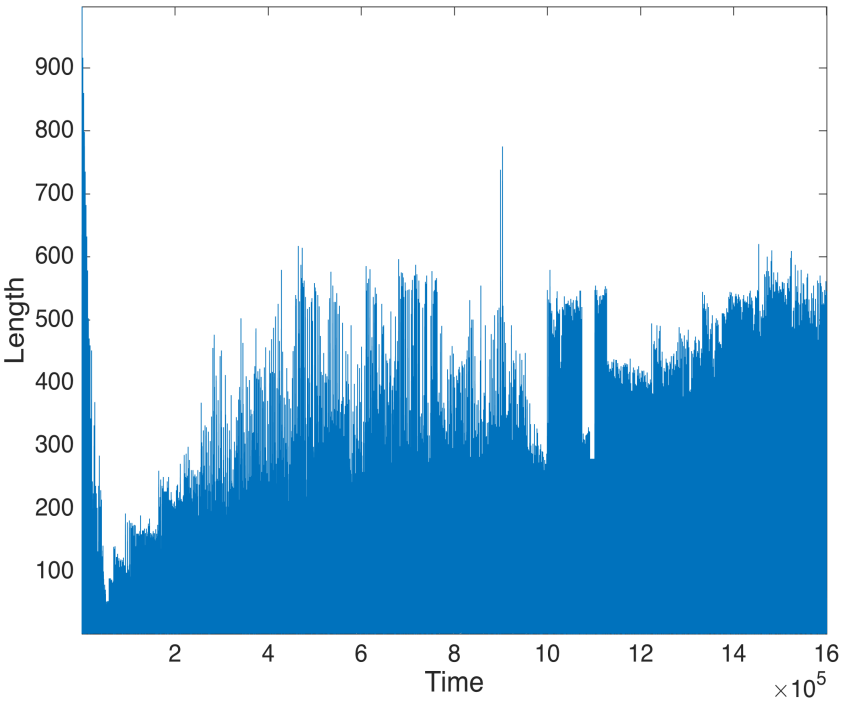

Figure 28: Event size distribution with water injection location at n=250:500.

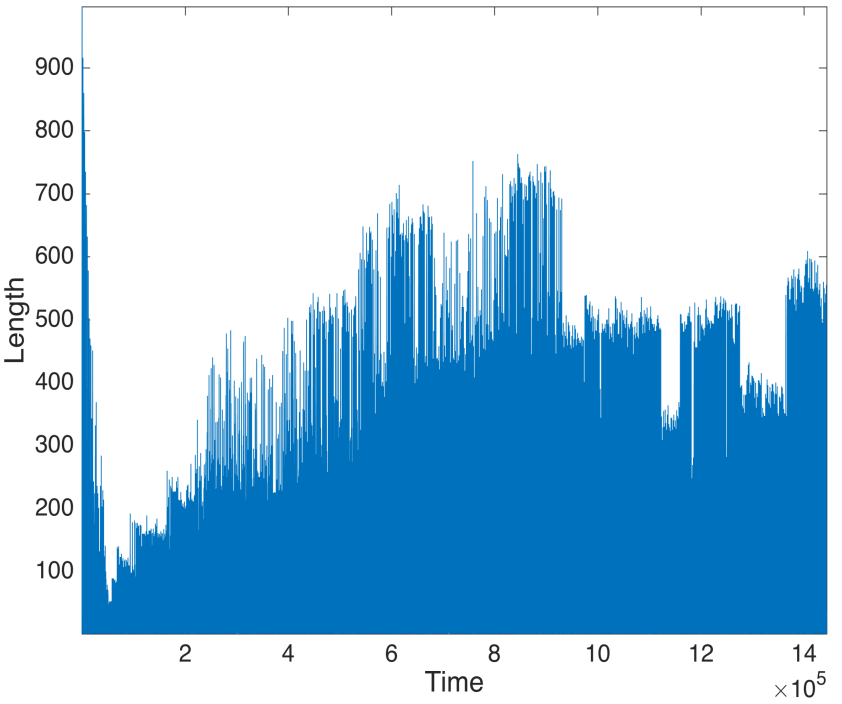

Figure 29: Event size distribution with water injection location at n=750:1000.

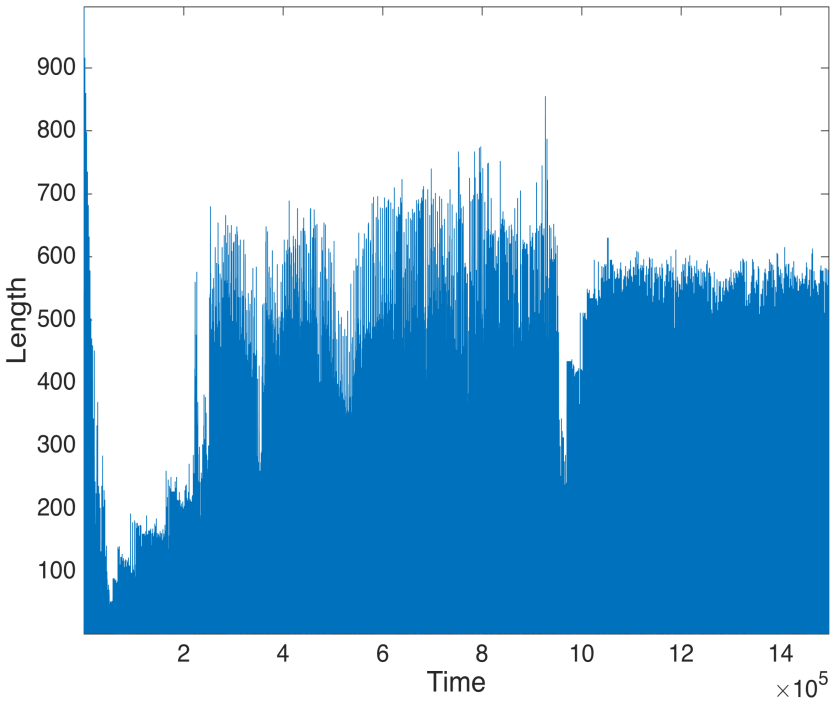

Figure 30: Event size distribution with water injection location at n=1:500.

4.5 Effects of water injection time on event size

In this section, we want to explore how the water injection time may impact on earthquake mechanism. In the one-dimension spring block model, we have the maximum event index 50,000. In the following cases, we change the starting time and ending time of stress reduction while keeping the reduction location and factor the same. Reduction factor is 0.5 and location is at the middle of the block chain. For the beginning water injection, we start the stress reduction at 1st event and end at the 10,000th, as Figure 31 is showed. For the early water injection, we start the stress reduction at 20,000th event and end at the 30,000th, as Figure 32 is showed. For the late water injection, we start the stress reduction at 30,000th event and end at the 40,000th, as Figure

33 is showed. In the case of inject-stop-inject, we firstly start start the stress reduction at 20,000th event and end at the 30,000th. Then, we continue the start the stress reduction at 30,000th event and end at the 40,000th. Figure 31 is the event size distribution for a beginning water injection. Comparing with Figure 21, which is the case without water injection, we can see that there are some extra events generated from the stress reduction in the beginning of the modeling. The event size from the stress reduction is about 300, less than one half of the blocks been moved. Figure 32 is the event size distribution for an early water injection. Medium events with an average event size about 400 are generated by stress reduction. For the late water injection, as shown in Figure 33, events generated by stress reduction is about 500 in scale. These three figures indicate that water injection time has an effect on the event size distribution. The later the stress reduction is subjected, the larger the events are generated. This could be explained that in the beginning of the modeling, events are still in the initiation stage where the chance of a large event is much smaller. Figure 34 is the case of inject-stop-inject where we have two injection periods in the system. From the plot, we can see there are two stages that event size increases and each of the stage correspond to a stress reduction period. The second stage generated larger event than the first as explained in the previous paragraph. Another finding is that after each stress reduction period, there is a sudden increase in the event size. Stress reduction has impact on the later events because the prestress in the system has been built up and thus, larger events could be generated.

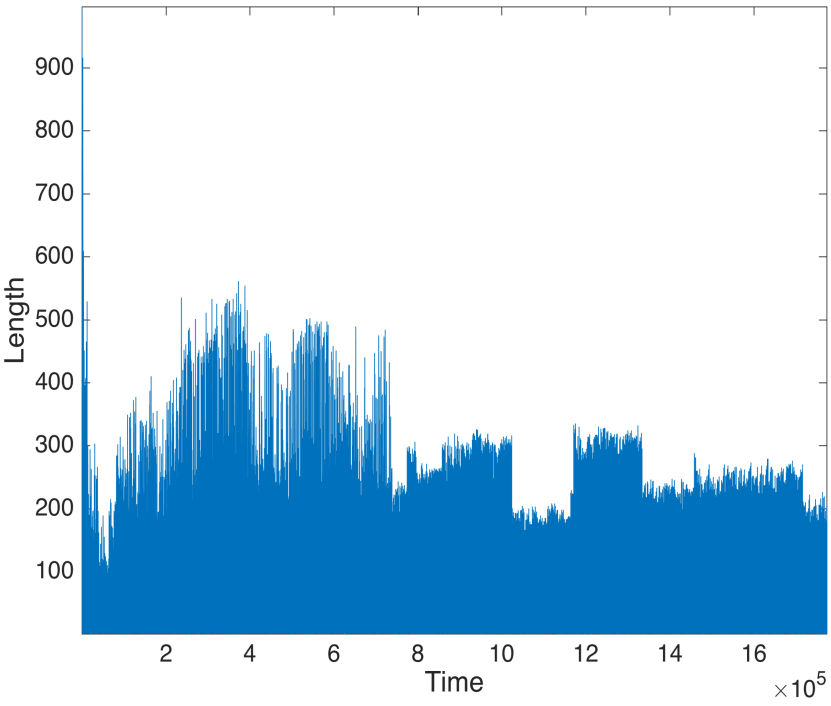

Figure 31: Beginning water injection event size distribution.

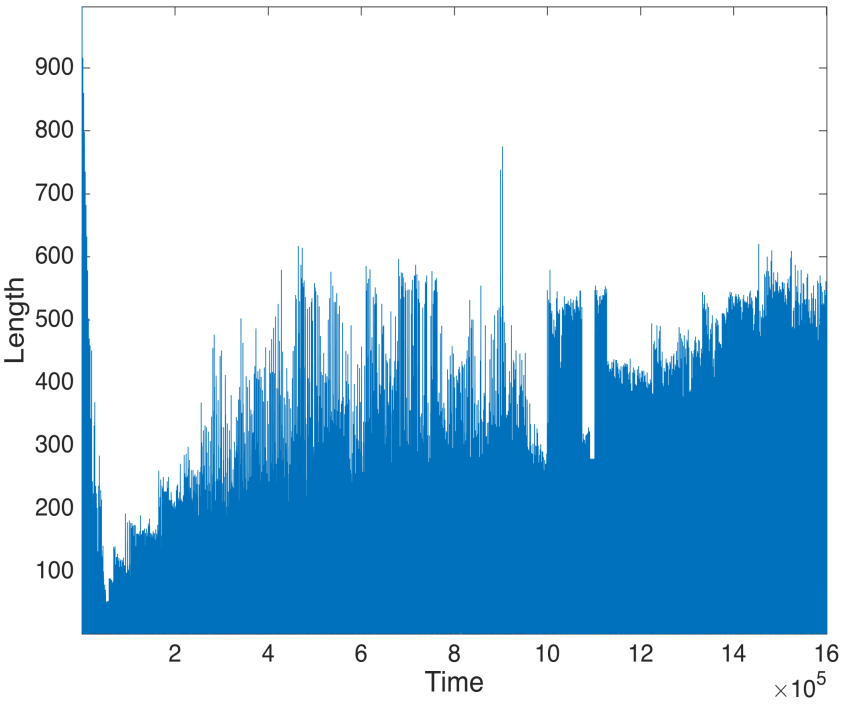

Figure 32: Early water injection event size distribution.

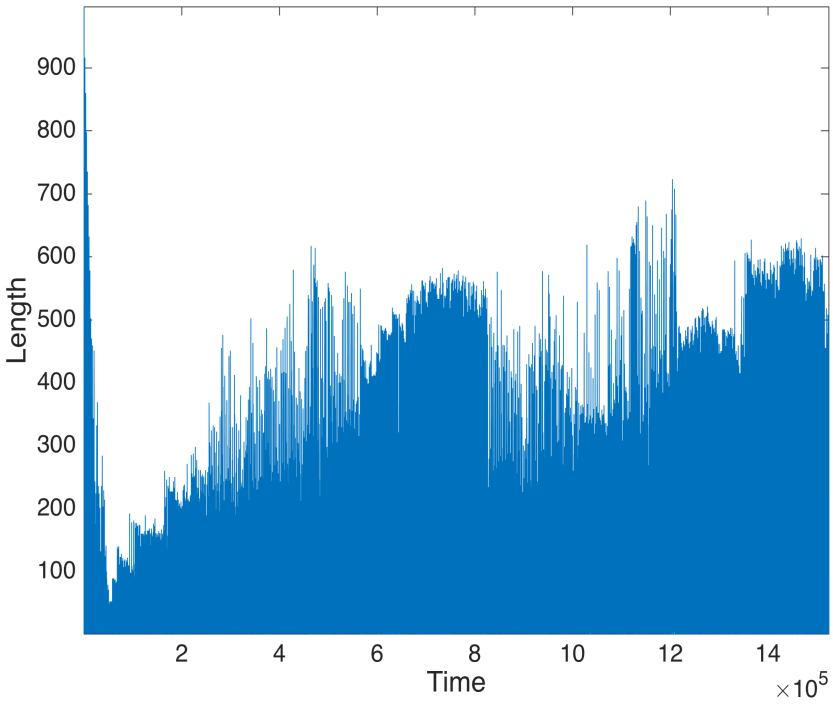

Figure 33: Injection-stop-injection event size distribution.

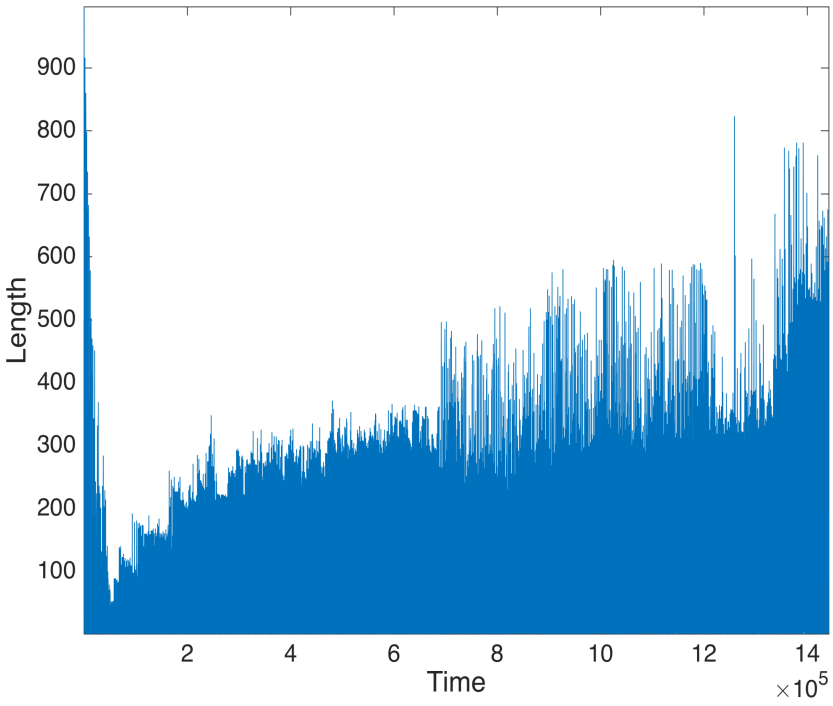

Figure 34: Late water injection event size distribution.

CHAPTER 5

DISCUSSION AND CONCLUSION

In conclusion, large events are likely to happen for stiff springs. Prestresses and energy are built up for a large event to happen. Heterogeneity is introduced by strong velocity weakening. An empirical relation is explored between average rupture stress and slip. The pulling force that drops and causes a large event is different for each case of spring stiffness. There are several directions to continue with the current study: firstly, we could further study the statistical properties of prestress to understand the self-organized or evolutionary behavior of 1D spring block model; secondly, we can expand 1D spring block model to 2D spring block model; and last but not least, apply 1D spring block model as an idealization of system for problems which requires complex dynamic analysis.

The wastewater injection and hydraulic fracturing have impacts on induced seismicity. Hydraulic fracturing and water injection could reduce the pore water pressure and thus, reduce the normal stress which is directly related with the velocity weakening friction. From our modelling, reduced stress at a certain location of blocks could generate more events. These generated events are mostly medium in size and the average rupture stress are smaller than the event without stress reduction. Moreover, water injection location and timing will also impact seismicity. Late water injection will generate larger events comparing to the early injection. Stress reduction at the end chain will also generate larger events than the front chain.

REFERENCES

[1] Burridge, R. and Knopoff, L., Bull. Seis. Soc. Amer. 57, 341, 1967. Carlson, J.M. and J.S.

[2] Carlson, J.M., Langer, J.S., Shaw, B.E., Tang, C., Intrinsic properties of a Burridge Knopoff model of an earthquake fault., Phys. Rev. A 44, 884–897 (1991).

[3] Elbanna, A.E.; "Pulselike Ruptures on Strong Velocity-Weakening Frictional Interfaces Dynamics and Implications" 2011.

[4] Erickson, B., B. Birnir and D. Lavallee, A Model for Aperiodicity in Earthquakes., Nonlinear Processes inGeophysics, 2008.

[5] Hough, Susan E.; Page, Morgan. "A Century of Induced Earthquakes in Oklahoma?". *10/20/2015*. U.S. Geological Survey. Retrieved

[6] Langer, Mechanical model of an earthquake fault, Phys. Rev. A 40, 6470–6484 (1989).

[7] Rice, J. R., Spatio-temporal complexity of slip on a fault, J. Geophys. Res., 98(B6), 9,885–9,907, 1993.

[8] U.S. Environmental Protection Agency (EPA). Washington, DC (2015-10-08). "General Information About Injection Wells"